

Magnifying Subtle Facial Motions for Effective 4D Expression Recognition

Qingkai Zhen

School of Computer Science and
Engineering, Beihang University, China
Email: qingkai.zhen@buaa.edu.cn

Di Huang

School of Computer Science and
Engineering, Beihang University, China
Email: dhuang@buaa.edu.cn

Yunhong Wang

School of Computer Science and
Engineering, Beihang University, China
Email: yhwang@buaa.edu.cn

Hassen Drira

Institut Mines-Télécom/Télécom Lille,
CRISAL (UMR CNRS 9189), France
Email: hassen.drira@telecom-lille.fr

Boulbaba Ben Amor

Institut Mines-Télécom/Télécom Lille,
CRISAL (UMR CNRS 9189), France
Email: boulbaba.benamor@telecom-lille.fr

Mohamed Daoudi

Institut Mines-Télécom/Télécom Lille,
CRISAL (UMR CNRS 9189), France
Email: mohamed.daoudi@telecom-lille.fr

Abstract—In this paper, an effective pipeline to automatic 4D Facial Expression Recognition (4D FER) is proposed. It combines two growing but disparate ideas in Computer Vision – computing the spatial facial deformations using tools from Riemannian geometry and magnifying them using temporal filtering. The flow of 3D faces is first analyzed to capture the spatial deformations based on the recently-developed Riemannian approach proposed in [1], where registration and comparison of neighboring 3D faces are led jointly. Then, the obtained temporal evolution of these deformations are fed into a magnification method in order to amplify the facial activities over the time. The latter, main contribution of this paper, allows revealing subtle (hidden) deformations which enhance the emotion classification performance. We evaluated our approach on BU-4DFE dataset, the state-of-art 94.18% average performance and an improvement that exceeds 10% in classification accuracy, after magnifying extracted geometric features (deformations), are achieved.

I. INTRODUCTION

Facial expressions are important non-verbal ways for human beings to communicate their feeling and affective states. In recent years, as a major topic of affective computing, Facial Expression Recognition (FER) has attracted increasing interests due to its potential in many applications, such as psychological analysis [2], transport security (driver fatigue), computer graphics, human-machine interaction, animation of 3D avatars *etc.*

Sun and Yin, the pioneers of 4D FER, tracked the change of a generic deformable model to extract a *Spatio-Temporal* (ST) descriptor of the face from dynamic sequences of 3D scans [3]. The vertex flow tracking was applied to each frame to form a set of motion trajectories of the 3D face video. The spatio-temporal features and two-dimensional HMM were used for classification. In [4], they proposed a tracking-model-based approach for vertex registration and motion trajectory estimation in 4D FER. The 2D intermediary generated through conformal mapping and a generic model adaptation algorithm were employed to establish the correspondence across frames. ST-HMM which incorporates 3D surface characterization was utilized to learn the spatial and temporal information of faces. Canavan *et al* [5] described the 3D dynamic surface by

the surface curvature-based shape-index information, and the surface features are characterized in local regions along the temporal axis. A dynamic curvature descriptors is constructed from local regions as well as temporal domains, and 3D tracking model based method was applied to locate the local regions across 3D dynamic sequences. Sandbach *et al* [6] exploited 3D motion-based features (*Free-Form Deformation*, FFD) between neighboring 3D facial geometry frames for FER. A feature selection step was applied to localize the features of each of the onset and offset segments of the expression. The HMM classifier was used to model the full temporal dynamics of each expression. In their another work [7], the entire expressive sequence is modelled to contain an *Onset* followed by an *Apex* and an *Offset*. Feature selection methods are applied in order to extract features for each of the onset and offset segments of the expression. These features are then used to train *GentleBoost* classifiers and build an HMM in order to model the full temporal dynamics of the expression.

Ben Amor *et al* [1], [8], [9] presented the facial by collections of radial curves, then Riemannian shape analysis was applied to quantify dense deformations and extract motion from successive 3D frames. Two different classification schema were performed, a HMM-based classifier and a mean deformation-based classifier. Xue *et al* [10] extracted local depth patch-sequences from consecutive expression frames based on the automatically detected facial landmarks. Three dimension discrete cosine transform (3D-DCT) is then applied on these patch-sequence to extract spatio-temporal features for facial expression dynamic representation. Berretti *et al* [11] presented a fully-automatic and real-time approach for 4D FER. A set of 3D facial landmarks were automatically detected firstly, the local characteristics of the face around those landmarks and their mutual distances were used to model the facial deformation. The work of Fang *et al* [12], [13] emphasized 4D face data registration and dense corresponding between 3D meshes along the temporal line, and a variant of *Local Binary Patterns on Three Orthogonal Plane* (LBP-TOP) was introduced for static and dynamic feature extraction to

predict expression labels.

Even though the performance of *FER* has been substantially boosted by 4D data in recent years, there still exist an unsolved problem, that is the reputed similar expressions are difficult to distinguish since the facial deformations are sometimes really slight [14]. To handle this issue, this paper present a novel and effective approach to amplify the subtle facial deformation, the contribution of the paper are two-folds:

- A comprehensive pipeline of spatio-temporal processing for effective facial expression recognition from 4D data.
- A method to amplify subtle movements on facial surfaces which contributes to distinguish similar expressions.

The rest of the paper is structured as follows. In section II the background of the used feature is introduced. The magnification of subtle facial deformation is introduced in Section III. Our comprehensive experimental study is presented in Section IV, followed in Section V we conclude the paper.

II. BACKGROUND ON DENSE SCALAR FIELDS

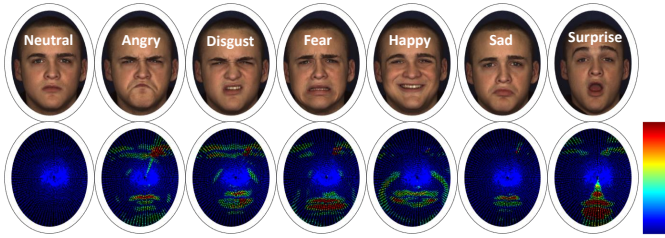


Fig. 1: Top row: facial texture images of an individual with different expressions. Bottom row: facial deformations in Riemannian space. Where, warm colors are associated to the high χ and correspond to facial regions with high deformations, cold colors reflect the most static parts of the 3D face.

Following the geometric approach recently-developed in [1], we represent 3D facial surfaces by collections of radial curves emanating from the tip of the nose. It is a new parameterization imposed for 3D face analysis, registration, comparison, *etc.* The amount of deformation from one shape into another (across the 3D video) is computed using tools from differential geometry through analyzing shapes of 3D radial curves as explained in the following. In the pre-processing step, the 3D mesh in each frame is first aligned to the first one and then cropped. The facial surfaces are then approximated by indexed collections of radial curves β_α , where the index α denotes the angle formed by the curve with respect to a reference radial curve. These curves are then uniformly resampled. Given a radial curve β of the face with an arbitrary orientation $\alpha \in [0, 2\pi]$, it can be parameterized as $\beta : I \rightarrow \mathbb{R}^3$, with $I = [0, 1]$, and mathematically represented using the SRVF, denoted by $q(t)$, according to:

$$q(t) = \frac{\dot{\beta}(t)}{\sqrt{\|\dot{\beta}(t)\|}}, t \in I. \quad (1)$$

This special representation has the advantage of capturing the shape of the curve and makes the calculus simpler. While there are several ways to analyze shapes of curves, an elastic analysis of the parametrized curves is particularly appropriate in our application – face analysis under facial expression variations. This is because (1) such analysis uses the square-root velocity function representation which allows us to compare local facial shapes in presence of deformations, (2) this method uses a square-root representation under which the elastic metric is reduced to the standard \mathbb{L}^2 metric and thus simplifies the analysis, (3) under this metric the group of re-parametrization acts by isometry on the curves manifold, thus a Riemannian re-parametrization metric can be set between two facial curves. Shown in Fig. 1 are examples of apex frames taken from the 3D videos of the BU-4DFE dataset as well as the dense 3D deformations computed with respect to the neutral frame. Let us define the space of the SRVFs as

$$\mathcal{C} = \{q : I \rightarrow \mathbb{R}^3, \|q\| = 1\} \subset \mathbb{L}^2(I, \mathbb{R}^3), \quad (2)$$

with $\|\cdot\|$ indicating the \mathbb{L}^2 norm. With the \mathbb{L}^2 metric on its tangent space, \mathcal{C} becomes a Riemannian manifold. Basically, with this parametrization each radial curve is represented on the manifold \mathcal{C} by its SRVF. Accordingly, given the SRVF q_1 and q_2 of two curves, the shortest path ψ^* on the manifold \mathcal{C} between q_1 and q_2 (called geodesic path) is a critical point of the following energy function:

$$E(\psi) = \frac{1}{2} \int \|\dot{\psi}(\tau)\|^2 d\tau, \quad (3)$$

where ψ denotes a path on the manifold \mathcal{C} between q_1 and q_2 , τ is the parameter for traveling along the path ψ , $\psi(\tau) \in T_{\psi(\tau)}(\mathcal{C})$ is the tangent vector field on the curve $\psi(\tau) \in \mathcal{C}$, and $\|\cdot\|$ denotes the \mathbb{L}^2 norm on the tangent space. Since elements of \mathcal{C} have a unit \mathbb{L}^2 norm, \mathcal{C} is an hypersphere in the Hilbert space $\mathbb{L}^2(I, \mathbb{R}^3)$. As a consequence, the geodesic path between any two points q_1 and $q_2 \in \mathcal{C}$ is given by the minor arc of the great circle connecting them. The tangent vector field on this geodesic between the curves β_1 and β_2 making the angle α with the reference curve is parallel along the geodesic and one can represent it with the initial velocity vector (called also shooting vector), without any loss of information.

$$\frac{d\psi_\alpha^*}{d\tau} \Big|_{\tau=0} = \frac{\theta}{\sin(\theta)}(q_2 - \cos(\theta)q_1), \quad (\theta \neq 0). \quad (4)$$

where $\theta = d_{\mathcal{C}}(q_1, q_2) = \cos^{-1}(\langle q_1, q_2 \rangle)$ represent the length of the geodesic path connecting q_1 to q_2 . In practice, the curves are re-sampled to a discrete number of points, say T , and the face is approximated by a collection of $|\Lambda|$ curves. The norm of the quantity at each discrete point r is computed to represent the amount of 3D deformations at each point of the surface parameterized by the pair (α, r) , termed Dense Scalar Fields (or *DSFs*). The final feature vector is of size $T \times |\Lambda|$. We will refer to this quantity at a given time t of the 3D video by $\chi(t)$ (see bottom row of Fig. 1 for illustrations). It provides the amplitude of the deformations between two facial surfaces in a dense way.

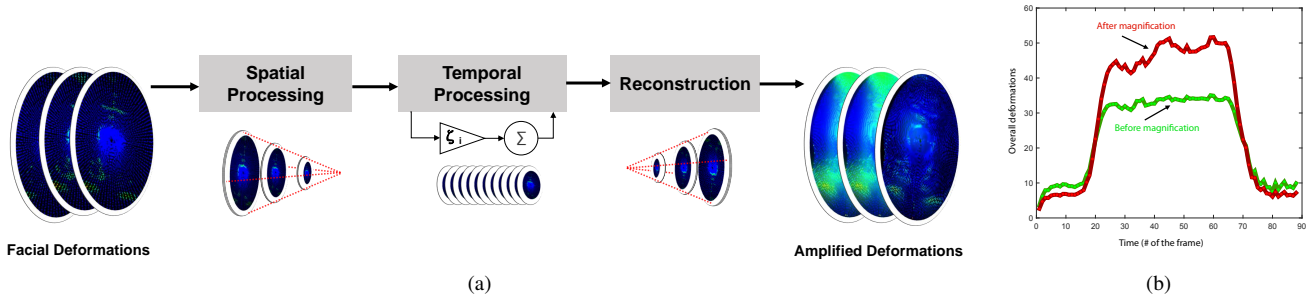


Fig. 2: (a) Overview of 3D video magnification. The original facial deformation features are first decomposed into different spatial frequencies, and the temporal filter is applied to all the frequency bands. The filtered spatial bands are then amplified by a given factor ζ , added back to the original signal, and collapsed to the output sequence. (b) An example of facial expression deformation (norm of the velocity vector) before (green) and after (red) magnification.

III. SUBTLE FACIAL DEFORMATION MAGNIFICATION

As described in Section II, χ reveals the shape difference of two facial surfaces by deforming one mesh into another through an accurate registration step. However, there exist another challenge to capture certain facial movements, especially the slight ones, with low spatial amplitude, reflected by the limited performance in distinguishing similar 3D facial expressions in the literature. To solve this problem, we propose a novel approach to highlight the subtle geometry changes of the facial surface in χ by adapting the Eulerian spatio-temporal processing [15] to the 3D domain. This method and its application to 3D face videos are presented in the subsequent. The Eulerian spatio-temporal processing was introduced for motion magnification in 2D videos, and has proved its effectiveness in [15]. Its basic idea is to amplify the variation of pixel values over time, in a spatially-multiscale manner, without explicitly estimating motion but rather exaggerating motion by amplifying temporal color changes at fixed positions. It relies on a linear approximation related to the brightness constancy assumption that forms the basis of the optical flow algorithm. However, the case is not that straightforward in 3D, because the vertex correspondence across frames cannot be achieved as easy as that in 2D. Fortunately, during the computation of χ , such correspondence is established by surface registration and remeshing. We can thus adapt Eulerian spatio-temporal processing to 3D face video. We take into account the values of the time series χ at any spatial location and highlight the differences in a given temporal frequency band of interest. It thus combines spatial and temporal processing to emphasize subtle changes in a 3D face video.

The process is illustrated in Fig. 2(a). Specifically, the video sequences are first decomposed into different spatial frequency bands by Gaussian pyramid, and these bands might be magnified differently. We consider that the time series correspond to the values of χ on the mesh surfaces in a frequency band and apply a band pass filter to extract the frequency bands of interest. The temporal processing, \mathfrak{T} , is uniform for all spatial levels, and for all χ within each level. We then multiply the extracted band passed signal by

a magnification factor ζ , and add the magnified signal to the original and collapse the spatial pyramid to obtain the final output.

Algorithm 1: Online 3D Deformation Magnification

Input: χ , l -Gaussian pyramid levels, ζ -amplification factor, ξ -sample rate, γ -attenuation rate, f -video frequency

Step1. Spatial Processing

for $i = 1; i \leq n$ **do**

$\mathfrak{D}(i, :, :, :) =$ decompose the $\chi(i)$, with l level Gaussian pyramid.

Step2. Temporal Processing

$\mathfrak{S} = \mathfrak{T}(\mathfrak{D}, f, \xi)$

Step3. Magnification

for $i = 1; i \leq 3$ **do**

$\mathfrak{S}(:, :, :, i) = \mathfrak{S}(:, :, :, i) * \zeta * \gamma$

Step3. Reconstruction

for $i = 1; i \leq n$ **do**

$\hat{\chi}(i) = \mathfrak{S}(i, :, :, :) + \chi(i)$

Output: $\hat{\chi}(t)$

For the translational motion of the facial mesh, we express the observed $\chi(s, t)$ value with respect to a displacement function $\delta(t)$, such that $\chi(s, t) = \chi(s) + \delta(t)$ and $\chi(s, 0) = \chi(s)$. By using a first-order Taylor series expansion, at time t , $\chi(s + \delta(t))$ in a first-order Taylor expansion about s , as

$$\chi(s, t) \approx \chi(s) + \delta(t) \frac{\partial \chi(s)}{\partial s} \quad (5)$$

Let $\phi(s, t)$ be the result of applying a broadband temporal band pass filter to $\chi(s)$ at each position (s). Assume that the motion signal $\delta(t)$ is within the pass band of the temporal band pass filter.

$$\phi(s, t) = \delta(t) \frac{\partial \chi(s)}{\partial s} \quad (6)$$

Amplify the band pass signal by factor ζ and add it back to $\chi(s)$.

$$\hat{\chi}(s, t) = \chi(s, t) + \zeta \phi(s, t) \quad (7)$$

By combining Eqn. 5, 6, and 7, we reach

$$\hat{\chi}(s, t) \approx \chi(s) + (1 + \zeta)\delta(t) \frac{\partial \chi(s)}{\partial s} \quad (8)$$

Assuming that the first-order Taylor expansion holds for the amplified larger perturbation $(1 + \zeta)\delta(t)$, the motion magnification of 3D face video can be simplified as follows:

$$\hat{\chi}(s, t) \approx \chi(s + (1 + \zeta)\delta(t)) \quad (9)$$

This shows that the spatial displacement $\delta(t)$ of the $\chi(s)$ at time t , is amplified to a magnitude of $(1 + \zeta)$. Sometimes $\delta(t)$ is not entirely within the pass band of the temporal filter. In this case, let $\delta_k(t)$, indexed by k , represent the different temporal spectral components of $\delta(t)$. This results in a band pass signal,

$$\phi(s, t) = \sum_k \gamma_k \delta_k(t) \frac{\partial \chi(s)}{\partial s} \quad (10)$$

where γ is an attenuation factor. Temporal frequency dependent attenuation can be equivalently interpreted as a frequency-dependent motion magnification factor, $\zeta_k = \gamma\zeta$, and the amplified output signal

$$\hat{\chi}(s, t) \approx \chi\left(s + \sum_k (1 + \zeta_k)\delta_k(t)\right) \quad (11)$$

this procedure, and Fig. 2(b) displays an example of facial deformation trajectory before (green) and after (red) magnification.

IV. EXPERIMENTAL RESULTS

A. Dataset Description and Experimental Settings

The BU-4DFE dataset [3] is a dynamic 3D facial expression dataset which consists of 3D facial sequences of 58 females and 43 males. It includes in total 606 3D sequences according to the 6 universal expressions. Each 3D sequence captures a facial expression at a rate of 25 fps (frames per second) and lasts approximately 3-4 seconds.

In our experiments, at a time t , the 3D face model f^t is approximated by a set of 200 elastic radial curves originating from the tip of the nose, a total of 50 sampled vertices on each curve is considered. Based on this parameterization, the 3D face shapes along the video sequence are compared to a reference frame f^0 to derive the $\chi(t)$ at each time t . Then, within the spatial processing step, a Gaussian pyramid decomposition is used to decompose χ into 4 band levels. Finally, a temporal processing to all the bands is applied. The factor ζ is set to 10, the sample rate ξ is set to 25, $f \in [0.3, 0.4]$, and the attenuation rate γ is set to 1. Our experiments are conducted on the following sub-pipelines – (1) the whole video sequence (denoted by *WV*), (2) the magnified whole video sequence (denoted as *MWV*).

A multi-class Support Vector Machine (*SVM*) is considered here where $\bar{\chi}$ is treated as a feature vector to predict the video label in the Subtle Deformation Magnification experiment (using *SVM Classifier*). We also adopt *HMM* to encode the temporal behavior of each expression, and get the expression type. To allow fair comparison with previous studies, we

randomly select 60 subjects from the BU-4DFE dataset to perform our experiments under a 10-fold cross-validation protocol.

B. Classification Performance

Table I provides a first summary of our results, it shows that the magnification procedure an improvement that exceeds 10% in classification accuracy is achieved. Before magnification, our approach achieves 82.49% and 83.19% as correct classification rate using *SVM* and *HMM* classifiers respectively, when consider full video. In particular, the *SU* and *HA* sequences are well classified with a high classification rate. This is mainly due to the high intensities and clear patterns of their deformations. However, remaining expressions (*DI*, *FE*, *AN* and *SA*) are harder to distinguish. We believe that two major reasons induce this difficulty: (1) the intra-class variability which makes confusing similar classes such as *DI/AN/FE*; (2) the low magnitude of the deformations exhibited when performing these expressions. After the magnification, the overall improvement exceeds 10% both all settings, which highlights the interest of the magnification procedure to reveal invisible deformations. It can be clearly seen from these confusion matrices, a significant improvement in distinguishing the *AN*, the *DI* and the *FE* expressions which have been difficult to recognize before. Table II shows the confusion matrices (*WV*, *MWV*) achieved by using *SVM* and *HMM* classifiers. Fig. 3 illustrations of the deformation magnification on sequences of the same subject.

C. Comparison with state-of-the-art

Several research groups have reported *FER* results on the BU-4DFE dataset, however they differ in their experimental settings. In this section, we compare our results with existing approaches when considering these differences.

Most of the results reported on BU-4DFE are shown in Table III. In this table, #E means the number of expressions, #S is the number of subjects, #-CV provides the number of cross-validation used, *Full Seq./Win* means the decision is made based on the analysis of the full sequence or on sub-sequences captured using a sliding window. The studies [3], [4] report one of the highest accuracy when using a sliding window of 6 frames, nevertheless, the approach requires manual annotation of 83 landmarks on the first frame. Moreover, the vertex-level dense tracking scheme is time consuming. In a more recent work from the same group developed by Reale *et al.* [16], the authors propose 4D (*Space-Time*) features termed *Nebula* computed on a fixed-size window of 15 frames. The best accuracy reported is 76.9% using sequences of 100 subjects, when the 3D video segmentation to limit the expressive time interval is performed manually. In [13], Fang *et al.* obtained an accuracy of 74.63% with 507 sequences of 100 subjects. Le *et al.* [17] evaluate their algorithm consisting of level curves and *HMMs* on 60 subjects sequences on three expressions (*HA*, *SA* and *SU*) and display an accuracy of 92.22%. It should be noted that the proposed approach is evaluated when considering full sequences which is a major difference to the works [3], [4],

TABLE I: Average accuracy (and standard deviations) achieved by *SVM* and *HMM* on *whole video sequence* before and after magnification.

Algorithm	Magnification?	Whole Sequence (%)
<i>SVM on $\bar{\chi}$</i>	N	82.49 ± 3.11
	Y	93.39 ± 3.54
<i>HMM on $\chi(t)$</i>	N	83.19 ± 2.84
	Y	94.18 ± 2.46

TABLE II: The confusion matrices (*WV*, *MWV*) achieved by using *SVM* and *HMM* classifiers.

SVM on $\bar{\chi}$	Whole Video (<i>WV</i>)						Magnified Whole Video (<i>MWV</i>)					
	%	AN	DI	FE	HA	SA	SU	AN	DI	FE	HA	SA
AN	73.86	9.18	6.49	1.75	6.11	2.51	91.07	2.73	2.01	1.59	2.08	0.51
DI	8.76	71.27	9.29	3.51	4.84	2.21	2.05	92.62	2.63	1.07	1.38	0.24
FE	5.79	5.37	73.14	4.59	5.39	5.61	1.66	1.53	92.33	1.31	1.54	1.62
HA	0.81	1.18	2.42	93.6	1.08	0.88	0.91	0.88	2.36	94.29	0.97	0.58
SA	2.54	2.27	2.99	1.63	88.75	1.77	1.36	1.22	1.62	0.9	93.93	0.96
SU	0.74	0.88	1.91	0.75	1.38	94.32	0.51	0.61	1.29	0.52	0.96	96.11
Average	82.49 ± 3.10						93.39 ± 3.54					
HMM on $\chi(t)$												
%	AN	DI	FE	HA	SA	SU	AN	DI	FE	HA	SA	SU
AN	75.29	5.88	7.31	1.14	8.17	2.21	91.87	1.91	2.41	0.38	2.69	0.73
DI	10.42	71.55	11.43	1.82	4.27	0.5	2.11	94.22	2.32	0.29	0.86	0.19
FE	5.07	6.86	73.69	3.33	8.06	2.99	1.37	1.86	92.85	0.91	2.19	0.81
HA	0.48	0.87	1.54	94.93	1.81	0.37	0.47	0.77	1.43	95.3	1.67	0.35
SA	3.71	1.01	4.17	0.65	89.19	1.26	1.84	0.51	2.07	0.33	94.61	0.63
SU	0.49	0.33	2.79	0.32	1.59	94.47	0.33	0.22	1.89	0.22	1.08	96.25
Average	83.19 ± 2.83						94.18 ± 2.46					

TABLE III: A comparative study of the proposed approach with the state-of-the-art on BU-4DFE.

Method	Experimental Settings	Accuracy
Sun <i>et al.</i> [3]	6E, 60S, 10-CV, Win=6	90.44%
Sun <i>et al.</i> [4]	6E, 60S, 10-CV, Win=6	94.37%
Reale <i>et al.</i> [16]	6E, 100S, -, Win=15	76.9%
Sandb. <i>et al.</i> [7]	6E, 60S, 6-CV, Win	64.6%
Fang <i>et al.</i> [13]	6E, 100S, 10-CV, -	74.63%
Le <i>et al.</i> [17]	3E, 60S, 10-CV, Full seq.	92.22%
Xue <i>et al.</i> [10]	6E, 60S, 10-CV, Full seq.	78.8%
Berretti <i>et al.</i> [11]	6E, 60S, 10-CV, Full seq.	79.4%
Berretti <i>et al.</i> [11]	6E, 60S, 10-CV, Win=6	72.25%
Ben Amor <i>et al.</i> [1]	6E, 60S, 10-CV, Full seq.	93.21%
Ben Amor <i>et al.</i> [1]	6E, 60S, 10-CV, Win=6.	93.83%
This work - SVM on $\bar{\chi}$	6E, 60S, 10-CV, Full seq.	93.39%
This work - HMM on $\chi(t)$	6E, 60S, 10-CV, Full seq.	94.18%

[16], [7]. It is pointed out in [11] that the problem of the window-based evaluation protocol is to label all sub-sequences from the neutral intervals as one of the six expressions which can bias the final result. Compared to the results listed in Table III, the proposed approach outperforms existing approaches, where (1) no landmark detection is required; (2) no dimensionality reduction or feature selection techniques are applied; and (3) A vertex-level 4D dense registration and quantification of the deformations are led jointly through a Riemannian approach. The temporal filtering amplifies these deformations

and consequently reveals hidden (subtle) 4D facial motions.

V. CONCLUSIONS

In this paper, a spatio-temporal processing approach for effective 4D *FER* is presented. It focus on an important issue – expression magnification to reveal subtle deformations. After a preprocessing step, the flow of 3D faces is analyzed to capture the spatial deformations based on the Riemannian method where registration and comparison are achieved jointly. Then, the obtained deformations are amplified using the temporal filter over the 3D face video. The combination of these two ideas performs accurate vertex-level registration of 4D faces and reveal hidden (subtle) deformations in 3D facial sequences. Experiments on BU-4DFE dataset demonstrate the effectiveness of the proposed method.

REFERENCES

- [1] B. Ben Amor, H. Drira, S. Berretti, M. Daoudi, and A. Srivastava, “4-d facial expression recognition by learning geometric deformations,” *IEEE Transactions on Cybernetics*, vol. 44, no. 12, pp. 2443–2457, 2014.
- [2] H. Meng, D. Huang, H. Wang, H. Yang, M. Al-Shuraifi, and Y. Wang, “Depression recognition based on dynamic facial and vocal expression features using partial least square regression,” in *International Workshop on Audio/Visual Emotion Challenge*, 2013, pp. 21–30.
- [3] Y. Sun and L. Yin, “Facial expression recognition based on 3d dynamic range model sequences,” in *European Conference on Computer Vision*, 2008, pp. 58–71.

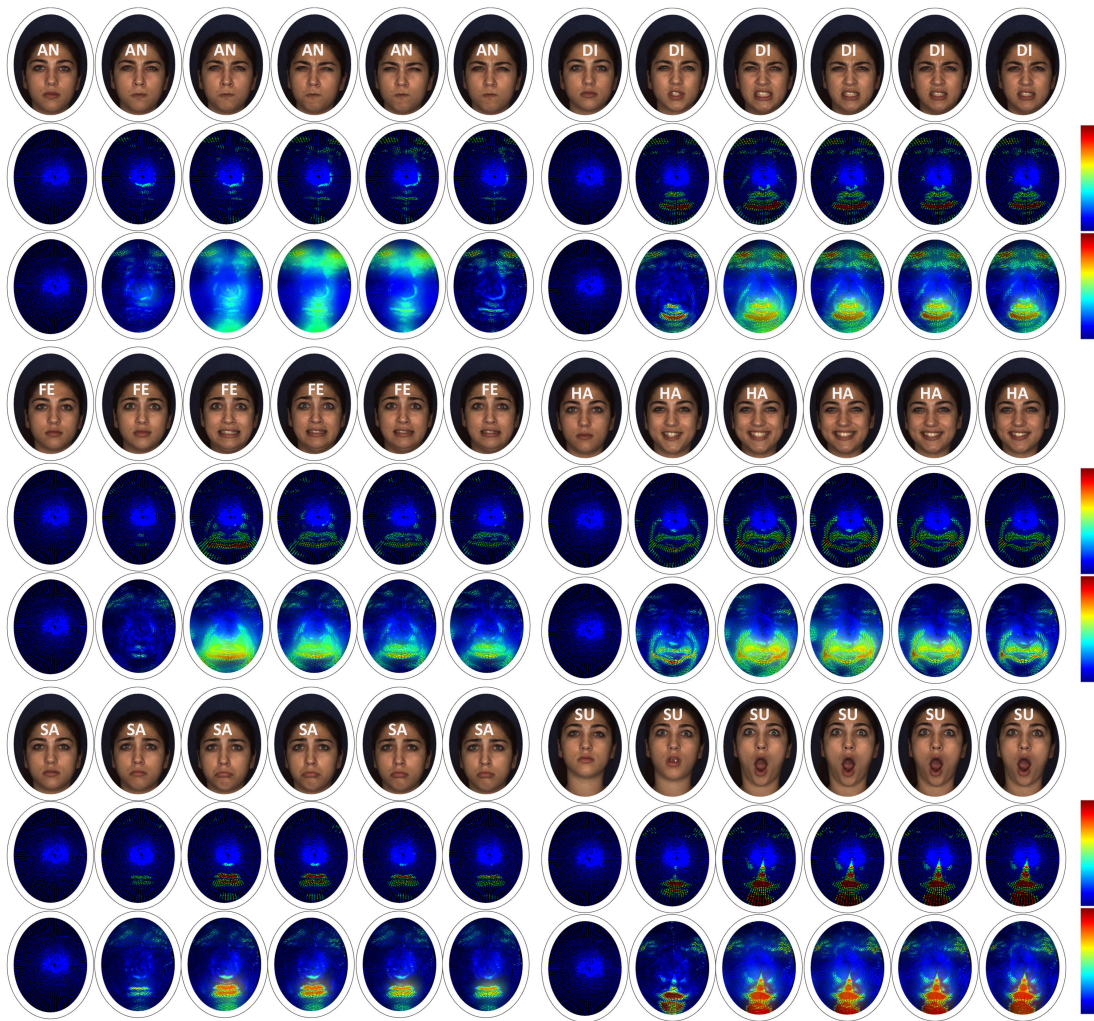


Fig. 3: Illustrations of the deformation magnification on sequences of the same subject performing six expressions. One can appreciate the magnification effects on 3D deformations compared to those of the original features. From up to bottom, each row presents the texture image, the original features, and the amplified features, respectively.

- [4] Y. Sun, X. Chen, M. Rosato, and L. Yin, "Tracking vertex flow and model adaptation for three-dimensional spatiotemporal face analysis," *IEEE Transactions on Systems, Man and Cybernetics, Part A: Systems and Humans*, vol. 40, no. 3, pp. 461–474, 2010.
- [5] S. Canavan, Y. Sun, X. Zhang, and L. Yin, "A dynamic curvature based approach for facial activity analysis in 3d space," in *Computer Vision and Pattern Recognition Workshops*, 2012, pp. 14–19.
- [6] G. Sandbach, S. Zafeiriou, M. Pantic, and D. Rueckert, "A dynamic approach to the recognition of 3d facial expressions and their temporal models," in *IEEE International Conference on Automatic Face Gesture Recognition and Workshops*, 2011, pp. 406–413.
- [7] —, "Recognition of 3d facial expression dynamics," *Image and Vision Computing*, vol. 30, no. 10, pp. 762–773, 2012.
- [8] H. Drira, B. B. Amor, M. Daoudi, A. Srivastava, and S. Berretti, "3d dynamic expression recognition based on a novel deformation vector field and random forest," in *International Conference on Pattern Recognition*, 2012, pp. 1104–1107.
- [9] M. Daoudi, H. Drira, B. B. Amor, and S. Berretti, "A dynamic geometry-based approach for 4d facial expressions recognition," in *European Workshop on Visual Information Processing*, 2013, pp. 280–284.
- [10] M. Xue, A. Mian, W. Liu, and L. Li, "Automatic 4d facial expression recognition using dct features," in *IEEE Winter Conference on Applications of Computer Vision*, pp. 199–206.
- [11] S. Berretti, A. Del Bimbo, and P. Pala, "Automatic facial expression recognition in real-time from dynamic sequences of 3d face scans," *The Visual Computer*, vol. 29, no. 12, pp. 1333–1350, 2013.
- [12] T. Fang, X. Zhao, S. K. Shah, and I. A. Kakadiaris, "4d facial expression recognition," in *IEEE International Conference on Computer Vision Workshops*, 2011, pp. 1594–1601.
- [13] T. Fang, X. Zhao, O. Ocegueda, S. K. Shah, and I. A. Kakadiaris, "3d/4d facial expression analysis: An advanced annotated face model approach," *Image and Vision Computing*, vol. 30, no. 10, pp. 738–749, 2012.
- [14] X. Yang, D. Huang, Y. Wang, and L. Chen, "Automatic 3d facial expression recognition using geometric scattering representation," in *IEEE International Conference on Automatic Face and Gesture Recognition and Workshops*, vol. 1, 2015, pp. 1–6.
- [15] H.-Y. Wu, M. Rubinstein, E. Shih, J. Guttg, F. Durand, and W. Freeman, "Eulerian video magnification for revealing subtle changes in the world," *ACM Trans. Graph.*, vol. 31, no. 4, pp. 1–8, 2012.
- [16] M. Reale, X. Zhang, and L. Yin, "Nebula feature: A space-time feature for posed and spontaneous 4D facial behavior analysis," in *IEEE International Conference on Automatic Face and Gesture Recognition*, 2013, pp. 1–8.
- [17] V. Le, H. Tang, and T. Huang, "Expression recognition from 3d dynamic faces using robust spatio-temporal shape features," in *IEEE International Conference on Automatic Face Gesture Recognition and Workshops*, 2011, pp. 414–421.

REFERENCES

- [1] B. Ben Amor, H. Drira, S. Berretti, M. Daoudi, and A. Srivastava, "4-d facial expression recognition by learning geometric deformations," *IEEE Transactions on Cybernetics*, vol. 44, no. 12, pp. 2443–2457, 2014.
- [2] H. Meng, D. Huang, H. Wang, H. Yang, M. Al-Shuraifi, and Y. Wang, "Depression recognition based on dynamic facial and vocal expression features using partial least square regression," in *International Workshop on Audio/Visual Emotion Challenge*, 2013, pp. 21–30.
- [3] Y. Sun and L. Yin, "Facial expression recognition based on 3d dynamic range model sequences," in *European Conference on Computer Vision*, 2008, pp. 58–71.
- [4] Y. Sun, X. Chen, M. Rosato, and L. Yin, "Tracking vertex flow and model adaptation for three-dimensional spatiotemporal face analysis," *IEEE Transactions on Systems, Man and Cybernetics, Part A: Systems and Humans*, vol. 40, no. 3, pp. 461–474, 2010.
- [5] S. Canavan, Y. Sun, X. Zhang, and L. Yin, "A dynamic curvature based approach for facial activity analysis in 3d space," in *Computer Vision and Pattern Recognition Workshops*, 2012, pp. 14–19.
- [6] G. Sandbach, S. Zafeiriou, M. Pantic, and D. Rueckert, "A dynamic approach to the recognition of 3d facial expressions and their temporal models," in *IEEE International Conference on Automatic Face Gesture Recognition and Workshops*, 2011, pp. 406–413.
- [7] ———, "Recognition of 3d facial expression dynamics," *Image and Vision Computing*, vol. 30, no. 10, pp. 762–773, 2012.
- [8] H. Drira, B. B. Amor, M. Daoudi, A. Srivastava, and S. Berretti, "3d dynamic expression recognition based on a novel deformation vector field and random forest," in *International Conference on Pattern Recognition*, 2012, pp. 1104–1107.
- [9] M. Daoudi, H. Drira, B. B. Amor, and S. Berretti, "A dynamic geometry-based approach for 4d facial expressions recognition," in *European Workshop on Visual Information Processing*, 2013, pp. 280–284.
- [10] M. Xue, A. Mian, W. Liu, and L. Li, "Automatic 4d facial expression recognition using dct features," in *IEEE Winter Conference on Applications of Computer Vision*, pp. 199–206.
- [11] S. Berretti, A. Del Bimbo, and P. Pala, "Automatic facial expression recognition in real-time from dynamic sequences of 3d face scans," *The Visual Computer*, vol. 29, no. 12, pp. 1333–1350, 2013.
- [12] T. Fang, X. Zhao, S. K. Shah, and I. A. Kakadiaris, "4d facial expression recognition," in *IEEE International Conference on Computer Vision Workshops*, 2011, pp. 1594–1601.
- [13] T. Fang, X. Zhao, O. Ocegueda, S. K. Shah, and I. A. Kakadiaris, "3d/4d facial expression analysis: An advanced annotated face model approach," *Image and Vision Computing*, vol. 30, no. 10, pp. 738–749, 2012.
- [14] X. Yang, D. Huang, Y. Wang, and L. Chen, "Automatic 3d facial expression recognition using geometric scattering representation," in *IEEE International Conference on Automatic Face and Gesture Recognition and Workshops*, vol. 1, 2015, pp. 1–6.
- [15] H.-Y. Wu, M. Rubinstein, E. Shih, J. Guttag, F. Durand, and W. Freeman, "Eulerian video magnification for revealing subtle changes in the world," *ACM Trans. Graph.*, vol. 31, no. 4, pp. 1–8, 2012.
- [16] M. Reale, X. Zhang, and L. Yin, "Nebula feature: A space-time feature for posed and spontaneous 4D facial behavior analysis," in *IEEE International Conference on Automatic Face and Gesture Recognition*, 2013, pp. 1–8.
- [17] V. Le, H. Tang, and T. Huang, "Expression recognition from 3d dynamic faces using robust spatio-temporal shape features," in *IEEE International Conference on Automatic Face Gesture Recognition and Workshops*, 2011, pp. 414–421.